Crystallization of Polypropylene at High Cooling Rates: Microscopic and Calorimetric Studies

S. A. E. Boyer,[1,2]* P. Robinson,[3†] P. Ganet,[4] J.-P. Melis,[5] J.-M. Haudin[1]

[1]*MINES ParisTech, Centre de Mise en Forme des Matériaux, UMR CNRS 7635, Sophia Antipolis, France*
[2]*MINES Douai, Département Technologie des Polymères et Composites & Ingénierie Mécanique, Douai, France*
[3]*PerkinElmer LAS, Beaconsfield, United Kingdom*
[4]*Catalyse, Marseille, France*
[5]*PerkinElmer SAS, Courtaboeuf, France*

Received 30 November 2011; accepted 30 November 2011
DOI 10.1002/app.36578
Published online in Wiley Online Library (wileyonlinelibrary.com).

ABSTRACT: The use of three different calorimeters made it possible to measure the overall kinetics of isotactic polypropylene in the α-phase in a wide temperature range. Original results concerning the growth rate of α spherulites were also obtained by optical microscopy by using a prototype hot stage developed in our laboratory. A new growth regime seems to exist at low crystallization temperature. The number of nuclei shows a smooth evolution with temperature with no rupture in the nucleation behavior in the low-temperature range. Combination of experimental results and an appropriate extrapolation procedure lead to an overall kinetics law valid in the whole domain of existence of the α-phase. This law is based on Ozawa's formalism. It will be used in polymer processing. © 2012 Wiley Periodicals, Inc. J Appl Polym Sci 000: 000–000, 2012

Key words: crystallization; polypropylene; high cooling rate; differential scanning calorimetry; optical microscopy

INTRODUCTION

Structure development is much more a key issue in polymer processing, with a view to master the final properties of the products. Among the phenomena involved, crystallization plays a major role. It generally occurs under complex, inhomogeneous, and coupled mechanical (flow and pressure), thermal (cooling rates and temperature gradients), and geometrical (contact with processing tools) conditions. Numerical simulation is a useful tool to understand and predict these coupled phenomena. It aims at describing the development of crystallization during the process, as well as predicting the subsequent morphologies and the final properties. It requires the introduction of a crystallization model into a computer code dedicated to a thermomechanical description of the process. Very often articles have focused only on the first point, i.e., the overall crystallization kinetics. The coupling between the thermomechanical model of the process and the crystallization kinetics is generally achieved through the energy equation, which takes into account the heat released by crystallization. The time dependence of this heat release is governed by the relative crystallinity, i.e., the ratio of the mass crystallinity at a given time t to the final crystallinity. For convenience, the relative crystallinity is usually assimilated to the volume fraction $\alpha(t)$ transformed into morphological entities of a given shape like spheres, although the two quantities are different in nature. Then, two types of problems have to be addressed: first, to choose a mathematical expression for $\alpha(t)$ and second, to determine the values of the physical parameters involved in this expression.

Most of the articles dealing with the introduction of a kinetic law for crystallization into models for polymer processing are based on the Avrami-Evans (AE) theory,[1–4] which gathers different approaches in fact equivalent after more in-depth analysis. To treat nonisothermal crystallization, simplifying additional assumptions have often been used, leading to analytical expressions, and allowing an easy determination of the physical parameters by differential scanning calorimetry (DSC). In the first place, one can mention the popular model of Nakamura,[5]

**Present address:* Institut P PRIME P', CNRS, ISAE-ENSMA, Université de Poitiers, UPR 3346, Futuroscope, France.
†*Present address:* Ruston Services Ltd., Stoke-on-Trent, United Kingdom.
This article was presented at the 4th International Conference on Polymer Behavior, International Union of Pure and Applied Chemistry, Lodz, Poland, September 20–23, 2010.
Correspondence to: S. A. E. Boyer (severine.boyer@ensma.fr) and J.-M. Haudin (jean-marc.haudin@mines-paristech.fr).
Contract grant sponsors: ARMINES, MINES-ParisTech, MINES-Douai.

which derives from a simplified form of Avrami's equation and has been widely used in polymer processing. Other authors preferred Ozawa's approach,[6] extended by Billon et al.[7] to nonconstant cooling rates. To avoid such simplifying assumptions, some authors[8,9] differentiated the general AE equation with respect to time and obtained a system of differential equations, more suitable for numerical simulation. These general approaches require a more sophisticated determination of the kinetic parameters by optical microscopy often combined with the measurement of the depolarized light intensity.[10,11]

The major experimental problem is that the maximum cooling rates available in classical commercial hot stages are limited to about 20°C/min. Consequently, to reach higher cooling rates, special devices are required. Very few are described in the literature.[12–16] They allow measurements in the 1000–5000°C/min range. Recently, Märtson et al.[17] designed a temperature-controlling cell for investigating the kinetics of fast phase transitions of polymers at high supercooling. The contact cooling rate of the hot stage can be increased up to 1000°C/s.

In the same way, till now DSC was in practice limited to cooling rates of several tens of °C/min. Mathot and coworkers[18–22] have shown that using a high-performance DSC apparatus (HPer DSC), DSC can be used at rates up to 500°C/min to study rate-dependent phenomena in real time. As a result of academic work and industrial development, it is now possible to work confidently with commercial equipments at several hundreds of °C/min. To attain higher cooling rates, an ultrafast thin film calorimeter, or nanocalorimeter, was proposed by Adamovsky, Schick and coworkers.[23–26] Rates higher than 1000°C/s and up to 100,000°C/s can be attained, both in cooling and in heating modes.

Because of the lack of experimental results, it has been often necessary to extrapolate the available data to reach the cooling rates actually obtained in some processes. Obviously, this graphical or numerical extrapolation may lead to erroneous results, from a physical point of view. Furthermore, it supposes that the crystallization phenomena, especially nucleation, remain the same at high cooling rates, which remains an open question. Such an extrapolation procedure has been applied to polypropylene to model structure development in the extrusion-coating process.[27] The model was able to predict structure development within the films and to give an interpretation of the adhesion properties in relationship with processing conditions. This can be considered as an *a posteriori* validation of the crystallization laws.

The purpose of this article is to revisit and to improve the extrapolation procedure used by Devisme et al.,[27] which derives from an initial proposal of Duffo.[28] A first route is to limit the extrapolation domain by acquiring data at higher cooling rates. By using new DSC facilities, a master curve has been established for the overall crystallization kinetics of isotactic polypropylene (iPP) in the α-phase, i.e., for cooling rates lower than about 100°C/s.[29] After discussion of the existing models, Ozawa's formalism has been retained. The values of the kinetic parameters have been determined from DSC data obtained with both classical and more recent equipment. Additional data on nucleation and growth at high cooling rates, i.e., at low crystallization temperatures, have been obtained with the prototype hot stage developed in our laboratory.[14–16] They will be used to propose various extrapolation methods. All the results will be compared to literature data, which leads to a consistent view of the crystallization of isotactic polypropylene in the α-phase.

THEORETICAL BRACKGROUND

General framework

The volume fraction $\alpha(t)$ transformed into morphological entities such as spheres can be described by different mathematical expressions which have been critically assessed by Piorkowska et al.[30,31] Most of them are based on the general equation derived from the AE theory:[1–4]

$$\alpha(t) = 1 - \exp[-\tilde{\alpha}(t)] \tag{1}$$

$\tilde{\alpha}(t)$ is the "extended" transformed fraction, which is calculated by ignoring the impingement of growing domains and including the "phantom" entities originating from nucleation attempts in already solidified areas. For spheres growing at a radial growth rate $G(t)$, $\tilde{\alpha}(t)$ is given by:

$$\tilde{\alpha}(t) = \frac{4\pi}{3} \int_0^t \left[\int_\tau^t G(u)du \right]^3 \frac{d\tilde{N}_a(\tau)}{d\tau} d\tau \tag{2}$$

where $d\tilde{N}_a(t)/dt$ is the "extended" nucleation rate.

Simplified expressions

In isothermal conditions, $G = \text{const.}$, and if the nucleation is either purely instantaneous ($d\tilde{N}_a(\tau)/d\tau = D\delta(\tau)$, δ being the Dirac delta function), or purely sporadic in time ($d\tilde{N}_a(t)/dt = \text{const.}$), eq. (2) assumes the form:

$$\tilde{\alpha}(t) = kt^n \tag{3}$$

where k is a temperature function dependent on the nucleation and growth rates; n is the Avrami exponent, which assumes integer values depending on the type of nucleation and the dimensionality of the

process. Nakamura et al.[5] have extended eq. (3) to nonisothermal crystallization:

$$\tilde{\alpha}(t) = \left[\int_0^t k(T)^{1/n} ds\right]^n = \left[\int_0^t K(T) ds\right]^n \tag{4}$$

where T is the time-dependent temperature.

For cooling at a constant rate $\dot{T}$ and the same types of nucleation as above (instantaneous or sporadic in time), Ozawa[6] has proposed the following expression:

$$\tilde{\alpha}(t) = \tilde{\alpha}(T, \dot{T}) = \frac{\chi(T)}{|\dot{T}^n|} \tag{5}$$

generalized by Billon et al.[7] to nonconstant cooling rate in the integral form:

$$\tilde{\alpha}(t) = \left[\int_0^t -\frac{d\chi^{1/n}(T)}{dT} ds\right]^n \tag{6}$$

where n is the Avrami exponent and $\chi(T)$ a temperature function. Ozawa-Billon's approach is formally equivalent to Nakamura's approach, since:

$$\frac{d\chi^{1/n}(T)}{dT} = -k^{1/n}(T) = -K(T) \tag{7}$$

General systems of differential equations

Schneider et al.[8] differentiated eq. (2) with respect to time and obtained a system of differential equations, called the "rate equations," enabling to create auxiliary functions $\phi_i(t)$ interrelated in the following way:

$$\phi_i(t) G(t) = \dot{\phi}_{i-1}(t) \tag{8}$$

for $i = 1$, 2, and 3. These functions are in the form:

$$\phi_0(t) = \frac{4\pi}{3} \int_0^t \left[\int_\tau^t G(u) du\right]^3 \frac{d\tilde{N}_a(\tau)}{d\tau} d\tau = \tilde{\alpha}(t) \tag{9a}$$

$$\phi_1(t) = 4\pi \int_0^t \left[\int_\tau^t G(u) du\right]^2 \frac{d\tilde{N}_a(\tau)}{d\tau} d\tau \tag{9b}$$

$$\phi_2(t) = 8\pi \int_0^t \left[\int_\tau^t G(u) du\right] \frac{d\tilde{N}_a(\tau)}{d\tau} d\tau \tag{9c}$$

$$\phi_3(t) = 8\pi \int_0^t \frac{d\tilde{N}_a(\tau)}{d\tau} d\tau = 8\pi \tilde{N}_a(t) \tag{9d}$$

The functions ϕ_0 and ϕ_1 describe the total volume and surface of all the spherulites, per unit of volume, neglecting, however, spherulite impingement and truncation while taking into account phantom spherulites. With the same assumptions, $\phi_2/8\pi$ and $\phi_3/8\pi$ represent the sum of radii and the number of spherulites in unit volume.

Haudin and Chenot[9] also differentiated eq. (2), with additional considerations on nucleation based on Avrami's work.[1,2] Active nuclei originate from potential nuclei that are activated at the frequency $q(t)$. These potential nuclei may disappear either by activation, or by absorption by a growing entity. Conversely, new potential nuclei may be generated during cooling. In the three-dimensional (3D) case, the authors arrive to a nonlinear system of seven differential equations with seven unknown functions:

$$\frac{dN}{dt} = -N\left(q + \frac{1}{1-\alpha}\frac{d\alpha}{dt}\right) + (1-\alpha)\frac{dN_0(T)}{dT}\frac{dT}{dt} \tag{10a}$$

$$\frac{d\alpha}{dt} = 4\pi(1-\alpha)G(F^2\tilde{N}_a - 2FP + Q) \tag{10b}$$

$$\frac{dN_a}{dt} = qN \tag{10c}$$

$$\frac{d\tilde{N}_a}{dt} = \frac{qN}{1-\alpha} \tag{10d}$$

$$\frac{dF}{dt} = G \tag{10e}$$

$$\frac{dP}{dt} = F\frac{d\tilde{N}_a}{dt} \tag{10f}$$

$$\frac{dQ}{dt} = F^2\frac{d\tilde{N}_a}{dt} \tag{10g}$$

with the initial conditions at time $t = 0$:

$$N(0) = N_0, \quad \alpha(0) = N_a(0) = \tilde{N}_a(0) = F(0) = P(0) = Q(0) = 0 \tag{11}$$

The main variables are N, α, N_a, and $\tilde{N}_a$ and three auxiliary functions F, P, and Q are added to get a first-order ordinary differential system. N and N_a are the number of potential and activated nuclei per unit volume at time t, respectively; $\tilde{N}_a$ is the "extended" number of activated nuclei per unit volume. The model predicts crystallization using three physical parameters: the initial density of potential nuclei N_0, the frequency of activation q of these nuclei, and the growth rate G.

DISCUSSION

The major advantage of the simplified expressions is that the Avrami exponent n and the time-dependent

function $k(T)$ or $\chi(T)$ can be determined by DSC in simple experiments. For Ozawa's model, the experiments are performed at constant cooling rates, which is a current way of operating the calorimeter. The treatment of the experimental results to extract the kinetic parameters n and $\chi(T)$ is well established and will be presented in a forthcoming section. In contrast to the simplified approaches, the use of the general AE formulation, either in its integral form [eq. (2)] or after derivation [eqs. (9)], requires the knowledge of two functions of time: the growth rate $G(t)$ and the "extended" nucleation rate $d\tilde{N}_a(t)/dt$. In fact, the time dependence of G is usually through temperature, as $T = T(t)$. Therefore, the growth rate is classically deduced from the increase of spherulite radius versus time during crystallization experiments at a fixed temperature. The same experiments performed by light microscopy give the number of spherulites nucleated as a function of time, which has then to be expressed per unit area or volume. Nevertheless, this actual nucleation rate, $dN_a(t)/dt$, does not give direct access to $d\tilde{N}_a(t)/dt$. The problem is often simplified assuming instantaneous nucleation. Concerning Haudin–Chenot's approach, nucleation is characterized by two parameters functions of temperature: N_0 and q. Procedures for determining these parameters have been designed by Monasse et al.[10] and Boyer et al.[11] They involve experiments combining optical microscopy and depolarized light measurements.

A major criticism of the simplified models is that the exponent value, n, determined experimentally for various polymers on the basis of DSC measurements is rarely in agreement with the predicted integer numbers. This is a convincing argument in favor of more sophisticated approaches. Nevertheless, as discussed in Piorkowska et al.,[30] n for isotactic polypropylene is generally close to 3, which is consistent with instantaneous nucleation and growth of spheres in 3D, and consequently corresponds to a physical reality.

Furthermore, the kinetic parameters $\chi(T)$ and n can be simply modified to take into account flow effects, as encountered in processing:[32]

$$\ln \chi(T, \dot{\varepsilon}) = \ln \chi(T) + f(\dot{\varepsilon}) \quad (12)$$

$$n(\dot{\varepsilon}) = n + g(\dot{\varepsilon}) \quad (13)$$

where $\dot{\varepsilon}$ is the strain rate (shear or elongation), and the functions $f(\dot{\varepsilon})$ and $g(\dot{\varepsilon})$ are deduced from experiments.

In conclusion, the future is obviously to develop more rigorous and physically based crystallization models, which requires important experimental efforts to measure the relevant parameters, but it must also be confessed that approximate expressions often give nice results, from an engineering and even scientific point of view.[27,30,32] Therefore, in continuity with previous work,[27] Ozawa's approach will be kept here. Two additional reasons are the following: (i) the polymer under investigation is isotactic polypropylene and Ozawa's model applies rather well to this polymer; (ii) the main part of the experimental work will be done by DSC.

EXPERIMENTAL

Material

The experimental work was done with an isotactic polypropylene supplied by Atofina (now Arkema, France) under the reference PPH 3250 MR1 (equivalent to PPH 9081, Total Petrochemicals, Féluy, Belgium). Its main molecular parameters are M_n = 42,500 g/mol, M_w = 213,000 g/mol, M_w/M_n = 5, melt flow index (MFI) = 25 g/10 min, and isotatic index = 0.97. The MFI was determined according to the ISO 1133 method under 230°C/2.16 kg conditions. This polymer is a grade for injection molding. It was chosen because it produces spherulites easily observable by optical microscopy and was already used in previous work.[10,11,14–16]

Differential scanning calorimetry

Three power-compensation calorimeters from PerkinElmer (PerkinElmer, Shelton, CT) were used according to the desired range of constant cooling rates, namely, a conventional DSC 7 for cooling rates up to 60°C/min (i.e., 1, 2, 5, 7, 10, 12, 20, 40, and 60°C/min), a Pyris 1 DSC for cooling rates up to 120°C/min (i.e., 60, 100, and 120°C/min), and a Diamond DSC for cooling rates up to 350°C/min (i.e., 200, 250, 300, and 350°C/min). Both the Pyris 1 and Diamond DSCs are equipped with the HyperDSC™ technique, which is the commercial version of HPer DSC introduced by Pijpers et al.[18] HPer DSC can run samples as fast as 500°C/min under control, measuring the real sample temperature. This was actually checked with our polypropylene using a low mass specimen (0.534 mg), as shown in Figure 1: the sample temperature closely follows the imposed program between 210 and 49°C.

The sample masses varied from 3–4 mg (Diamond) to 11.2 mg (Pyris 1 and DSC 7). The DSCs were calibrated for temperature and enthalpy using high purity indium and lead. The thermal protocol was: (i) heating to 210°C at 10°C/min, (ii) holding at 210°C for about 90 s to erase the thermal history while avoiding polymer degradation, (iii) cooling at various constant cooling rates $\dot{T}$ down to 30°C. The system baseline was checked before and after the measurements.

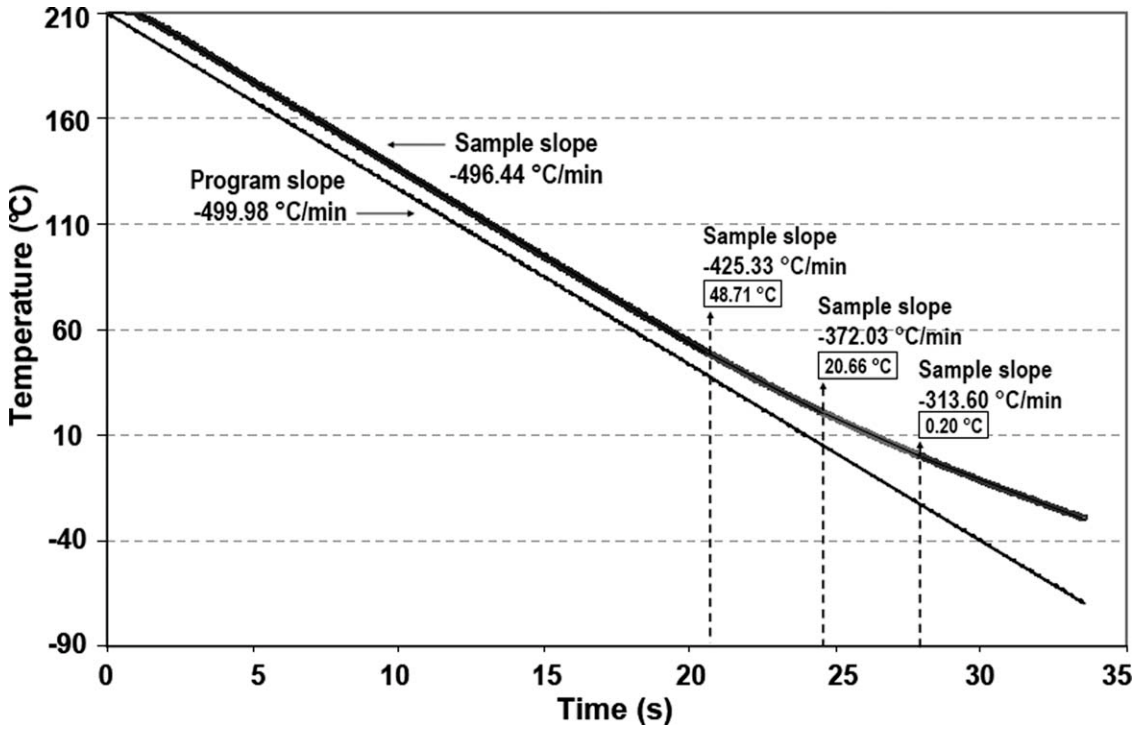

Figure 1 Comparison between program temperature and sample temperature during a programmed cooling at 500°C/min in a Diamond DSC. The actual cooling rates (slopes of the temperature versus time curves) are indicated. Sample mass: 0.534 mg.

Optical microscopy

A prototype hot stage named « Polymer High Cooling—Optics » has been especially designed to follow-up on-line the nucleation and growth of crystallizing entities at high cooling rate. The experimental setup is described in details elsewhere.[16] The polymer is placed into a "home-made" hot-stage chamber connected with a heating/cooling line and mounted into a light-depolarizing microscope. Sample temperature is continuously measured using a thermocouple embedded into the polymer.

The sample is heated and cooled down by a gaseous flowing heat transfer medium. The thermocouple is used to control its temperature by monitoring hot and cold air fluxes. When the cooling process begins, the hot air can be mixed or not with cold air according to three cooling modes: (I) proportional, (II) "all-or-none," and (III) "all." In the proportional mode (I), a throttle chamber receives the gaseous streams coming both from the heating and the cooling lines. The rate of mixing is controlled by the partial obstruction of the hot and cold air ducts using a ceramic rotating valve driven by a stepping motor. This procedure allows us to impose constant moderate cooling rates from 30 to 500°C/min. In the "all-or-none" mode (II), hot and cold fluxes are directly mixed in the hot-stage chamber. An "open-closed" valve is used to control the cold flux entering the hot-stage chamber, the hot flux being still controlled by the rotating mixing valve. Constant high cooling rates up to 1500°C/min are attained. In the "all" mode (III), cold air is directly injected into the hot stage, the hot line being completely closed. It permits to attain the highest cooling rates, but temperature variation is no longer linear with time.

The setup allows following the entities at the spherulitic scale, using a Leica-DMRX microscope (Leica-Microsystèmes, France) with an attached camera. The thermal polymer protocol is: (i) before crystallization, rapidly heating to about 215° C, (ii) holding at 215° C for about 90 s to erase the thermal history while avoiding oxidative degradation, enabling thus the processing of the sample for many cycles, (iii) cooling from 215 to 50°C at a constant cooling rate $\dot{T}$.

RESULTS AND DISCUSSION

DSC

During crystallization at constant cooling rate, the DSC records the heat power liberated by crystallization as a function of time or temperature. Time or temperature integration and normalization by the total heat of crystallization give the relative crystallinity as a function of time t or temperature T, which will be, as usual, assimilated to the volume fraction α transformed into semicrystalline entities. The α versus T curves obtained with the three calorimeters are

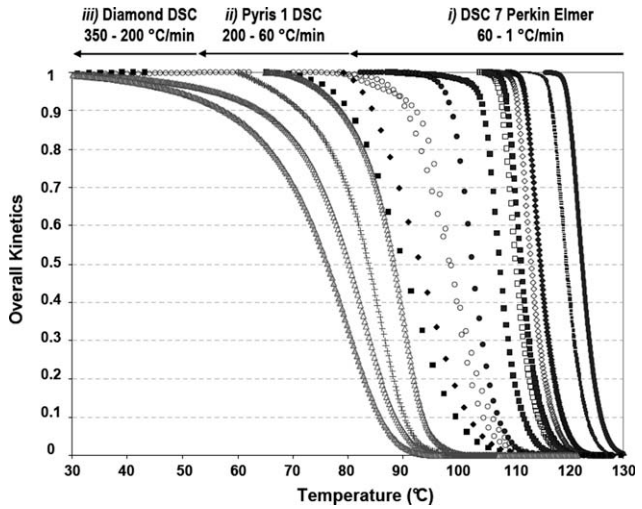

Figure 2 Overall kinetics (transformed volume fraction α) versus temperature obtained from the three power-compensation calorimeters. Cooling rates: (i) DSC 7: 1, 2, 5, 7, 10, 12, 20, 40, and 60°C/min, (ii) Pyris 1: 60, 100, and 120°C/min, (iii) Diamond: 200, 250, 300, and 350°C/min.

gathered in Figure 2. Despite the use of different apparatus, they show a consistent evolution of the kinetic curves. Logically, the $\alpha(T)$ curves are shifted to lower temperatures when the cooling rate increases.

The experimental overall kinetics obtained by DSC is generally described using Ozawa's eqs. (1) and (5), which can be cast into:

$$\ln\left(\ln\left(1-\alpha(T,\dot{T})\right)\right) = \ln\left(\chi(T)\right) - n\ \ln\left(\left|\dot{T}\right|\right) \qquad (14)$$

Therefore, the plot of $\ln\left(\ln\left(1-\alpha(T,\dot{T})\right)\right)$ against $\ln\left(\left|\dot{T}\right|\right)$ at given T should be in the form of set of straight lines having a slope $-n$. Such a plot has been done for α varying from 0.05 to 0.7 and is displayed in Figure 3. Because of the limited number of cooling rates available in practice in DSC experiments, it appears at each temperature as a linear segment or a succession of linear segments, each succession being approximated by a unique straight line. The slopes of these straight lines give the values of n, which are plotted as a function of temperature in Figure 4. It leads to an average value of $n = 2.58 \pm 0.26$. Similar values are described in the literature for isothermal and nonisothermal crystallization, e.g., 2.85 in the 107–130°C temperature range,[30] 2.69 ± 0.03 in the 120–132°C range,[33] 2.5 ± 0.1 at 136°C.[34] More generally, the Avrami exponent for iPP is found close to 3 (for a review, see Hieber[35]). It corresponds to instantaneous nucleation and growth of spheres in 3D, which justifies the use of Ozawa's approach.

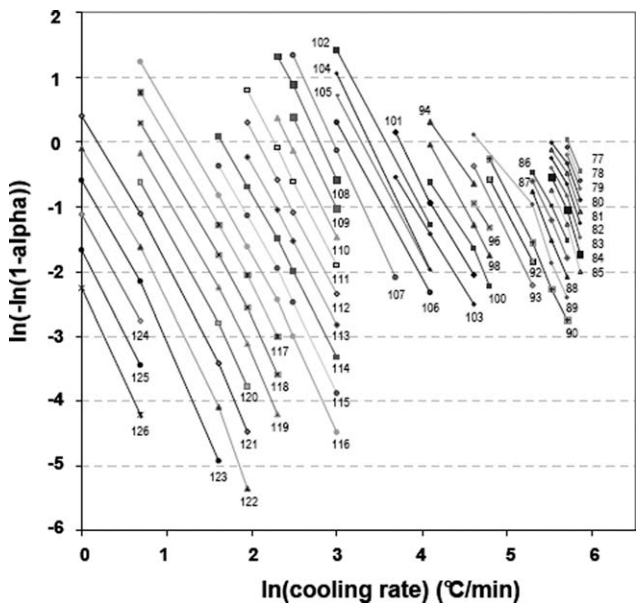

Figure 3 Plot of $\ln\left(\ln\left(1-\alpha(T,\dot{T})\right)\right)$ versus $\ln\left(\left|\dot{T}\right|\right)$ at given T.

Then, assuming $n = 3$ and using eq. (14), the $\ln\left(\chi(T)\right)$ function is determined as the master curve of the results obtained for the different cooling rates, which are superposed in Figure 5(A). It is correctly fitted in Figure 5(B) by the polynomial expression:

$$\ln\left(\chi(T)\right) = AT^4 + BT^3 + CT^2 + DT + E \qquad (15)$$

with T in °C and χ in $(°C/s)^3$. $A = 7.48 \times 10^{-8}$, $B = -7.17 \times 10^{-5}$, $C = 1.05 \times 10^{-2}$, $D = -6.14 \times 10^{-1}$, $E = 19.72$. To check the validity of this approach, the $\alpha(T)$ curves for different $\dot{T}$ are calculated from eqs. (1), (5), and (15) with $n = 3$, and compared to experimental ones in Figure 6. To fit the experimental curves with accuracy, a number of digits greater than that indicated above for A, B, C, D, and E is necessary because of the exponential form of the law. The agreement can be considered as good. The discrepancy observed at the end of crystallization at the highest cooling rates can be attributed to secondary crystallization. The lower slope of the experimental curve at 100°C/min could be related to low experimental values of n, close to 2, in this temperature range, as can be shown in Figure 4.

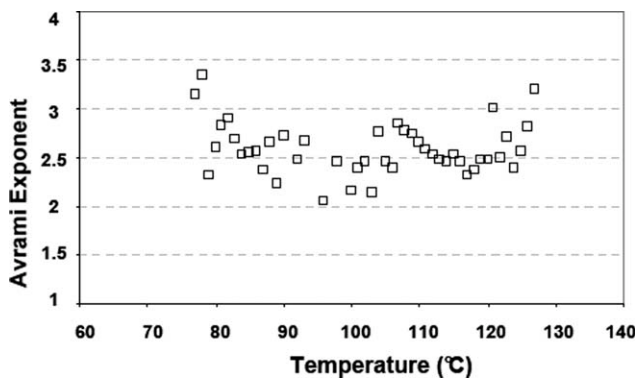

Figure 4 Avrami exponent versus temperature.

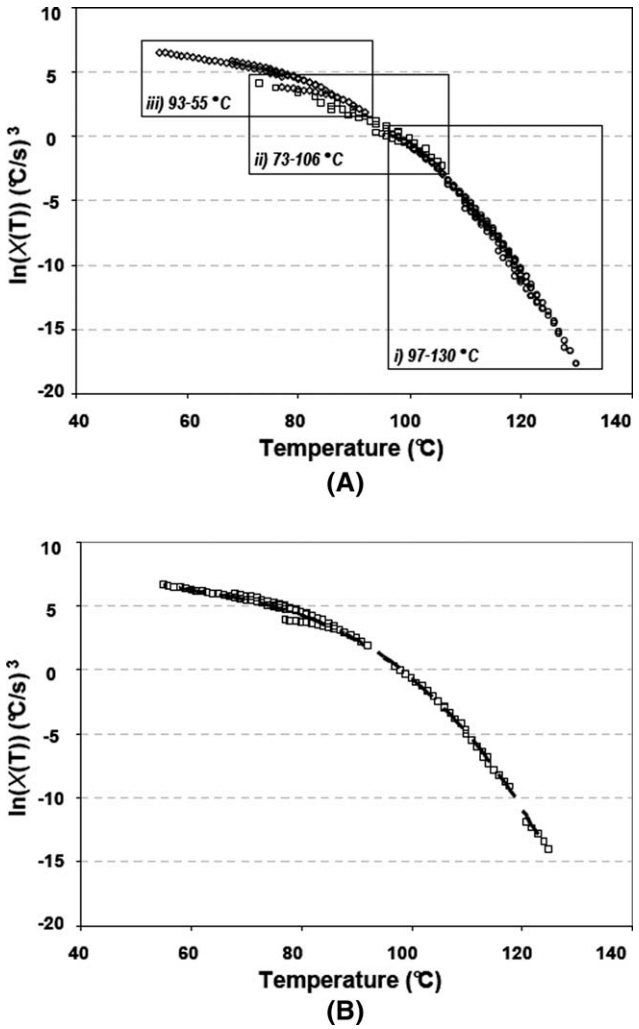

Figure 5 $\ln(\chi(T))$ versus temperature T: (A) experimental points; (B) dashed line: fit by the polynomial expression $\ln(\chi(T)) = AT^4 + BT^3 + CT^2 + DT + E$ with T in °C and χ in $(°C/s)^3$. $A = 7.48 \times 10^{-8}$, $B = -7.17 \times 10^{-5}$, $C = 1.05 \times 10^{-2}$, $D = -6.14 \times 10^{-1}$, and $E = 19.72$.

Hieber[35] has collected many kinetic data concerning the crystallization of iPP both in isothermal and nonisothermal conditions and proposed master curves to describe the overall kinetics. The parameters used, $\mathrm{Log}(\sigma(T))$ and $\mathrm{Log}(\lambda(T))$ with Log denoting the decimal logarithm, can be calculated from $\ln(\chi(T))$, with $\chi(T)$ in $(°C/s)^3$, by the following expressions:

$$\mathrm{Log}(\sigma(T))\ (^{\circ}\mathrm{C/min}) = \frac{\ln 60 + \frac{1}{n}\ln\chi(T)}{\ln 10} \quad (16)$$

$$\lambda(T)\,(\mathrm{min}) = \frac{k(T)^{-1/n}}{60} \quad (17)$$

where $k(T)^{1/n}$ in s is calculated by eq. (7). The results of our calculations are compared to Hieber's data in Figure 7(A,B). The agreement with its master curves is very good. Our work usefully completes Hieber's one in the low-temperature range, where the experimental results were scarce, especially for nonisothermal crystallization, as shown in Figure 7(A). For isothermal crystallization, the only points between 60 and 90°C in Hieber's article correspond to results of Magill,[36] obtained by polarized light microscopy. Experimental data in the same range were also obtained by De Santis et al.[37] using isothermal nanocalorimetry. The three sets of data are compared in Figure 7(B): they are in good agreement around 80°C, but some divergence occurs at lower temperature.

Optical microscopy

Growth rate

Growth rates were measured with our new apparatus « Polymer High Cooling—Optics ». The growth kinetics was calculated from the evolution of spherulite radii as a function of time. This evolution was followed during a time interval carefully selected for each cooling rate to obtain a linear variation of the radius. For each interval, the spherulite growth rate was thus determined, and the corresponding crystallization temperature was calculated as the mean temperature in the selected interval. For each cooling mode, this calculation was made by selecting three clearly identified spherulites, and a mean value of the growth rate was retained. Figure 8(A) gives the growth rate G of iPP spherulites against the crystallization temperature T_c. These spherulites correspond to the α-crystalline phase. Results obtained isothermally or at a low cooling rate using a conventional Mettler hot stage are also plotted to extend the curve to higher temperature. Therefore, it is possible to collect many growth-rate data for the same polymer in a wide range of temperature, from 57 to 158°C. Our results are compared in Figure 8(B) with those of Nakamura et al.[38] and with the data collection from Janeschitz-Kriegl.[39] A good agreement can be observed between the three sets of data.

Hoffman and Lauritzen proposed and repeatedly revisited a kinetic theory of growth based on a mechanism of secondary nucleation.[40–43] They distinguish three different modes of lamellar growth, called Regimes I, II, and III, respectively. These regimes differ by the deposit mechanisms of molecular stems on the growth front or, in other words, by the relative values of the secondary nucleation rate on the substrate and of the substrate completion rate. Regime I is observed for high crystallization temperature where one surface nucleus causes the completion of the entire substrate;

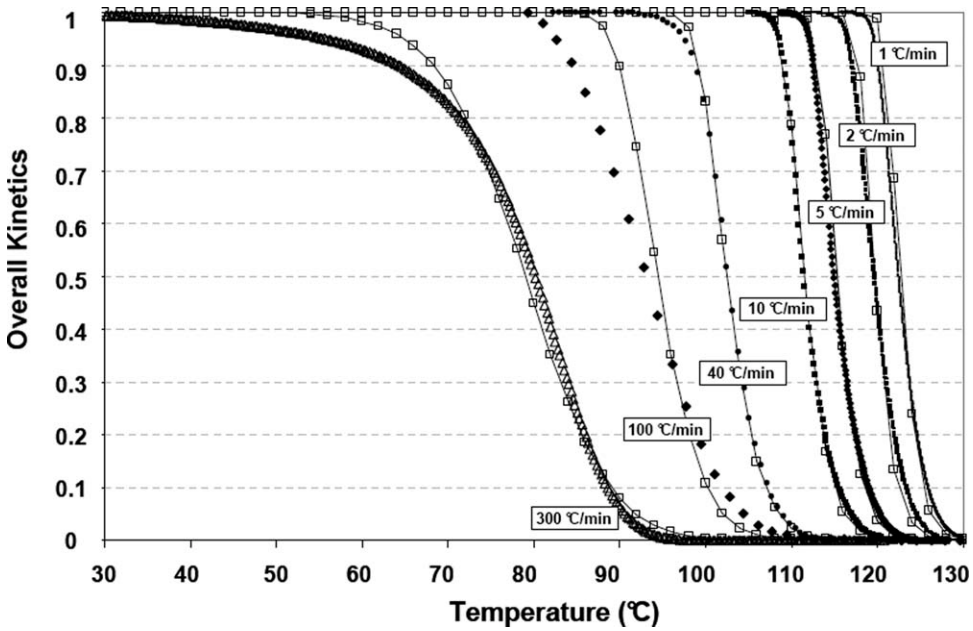

Figure 6 Comparison between overall kinetics for different $\dot{T}$ calculated from eqs. (1), (5), and (15) with $n = 3$ (full lines with squares), and experimental ones.

Regime II is observed when multiple surface nuclei begin to occur on the substrate because of a larger undercooling; Regime III is similar to Regime II, but is entered when the mean separation of the nuclei on the substrate approaches the width of a molecular stem. For these three regimes, the growth rate G of a crystalline entity (e.g., spherulite) is described by the general expression:

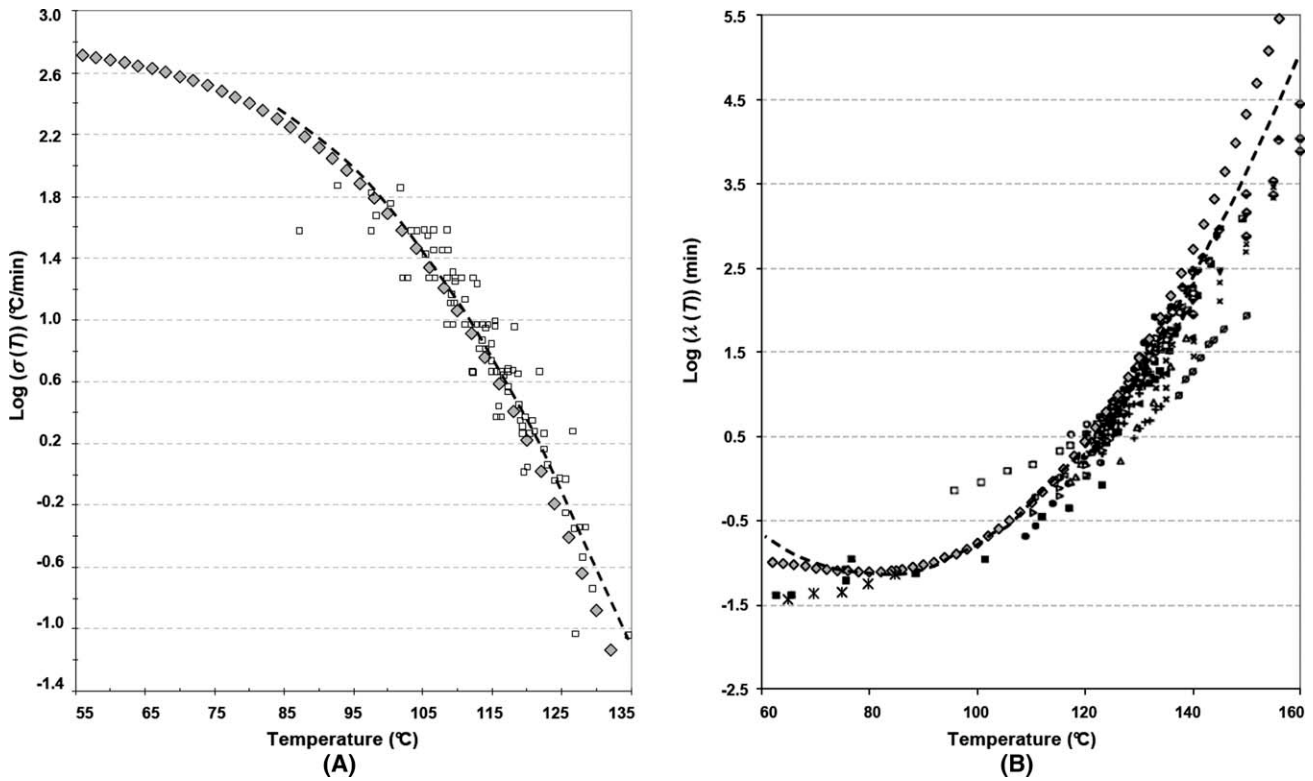

Figure 7 Comparison between our experimental results (closed diamonds) and the data collected by Hieber.[35] The parameters used are defined in the text: (A) constant cooling-rate crystallization; (B) isothermal crystallization. The black squares come from the article of Magill.[36] The results of De Santis et al.[37] have also been plotted (*).

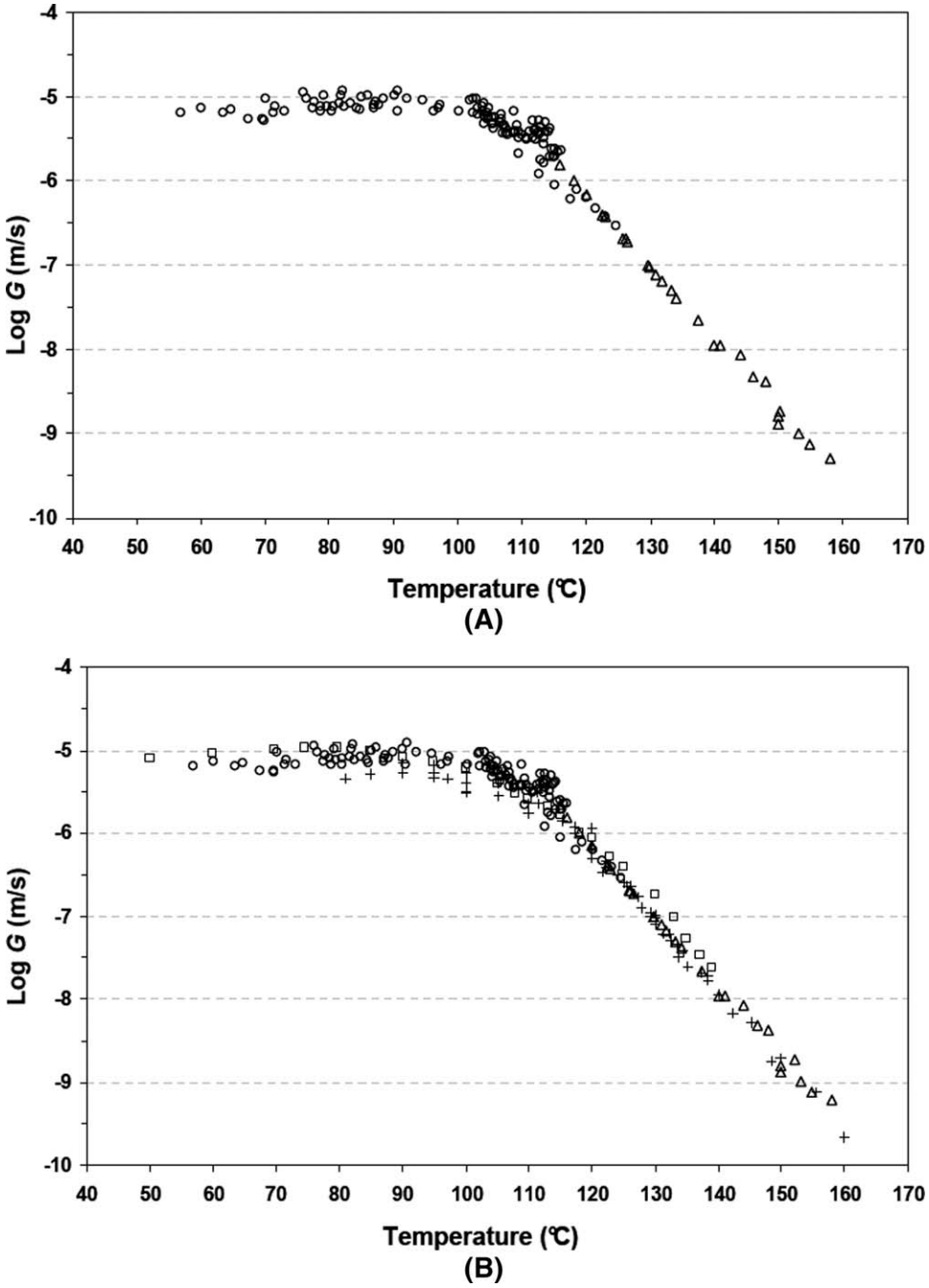

Figure 8 Decimal logarithm of the growth rate G of iPP spherulites against the crystallization temperature T_c: (A) experimental results in isothermal (triangles) and nonisothermal conditions (circles); (B) comparison with the results of Nakamura et al.[38] (squares) and with the data collection from Janeschitz-Kriegl[39] (crosses).

$$G(T_c) = G_0^i \exp\left(-\frac{U^*}{R\,(T_c - T_\infty)}\right) \exp\left(-\frac{K_g^i}{T_c\,(T_m^0 - T_c)}\right) \tag{18}$$

T_c is the crystallization temperature, and ΔT is the degree of undercooling: $\Delta T = T_m^0 - T_c$, with T_m^0 the equilibrium melting temperature. U^* is the activation energy for the transport of molecular segments across the melt/crystal interface and T_∞ is the temperature at which molecular mobility ceases. Usually, $U^* = 6270$ J/mol and $T_\infty = T_g - 30$, T_g being the glass transition temperature. R is the gas constant, equal to 8.314 J/mol/K. G_0^i and K_g^i are constant for a given regime (i = I, II, III).

Equation (18) can be rewritten as:

$$\ln G + \frac{U^*}{R(T_c - T_\infty)} = \ln G_0^i - \frac{K_g^i}{T_c(\Delta T)} \tag{19}$$

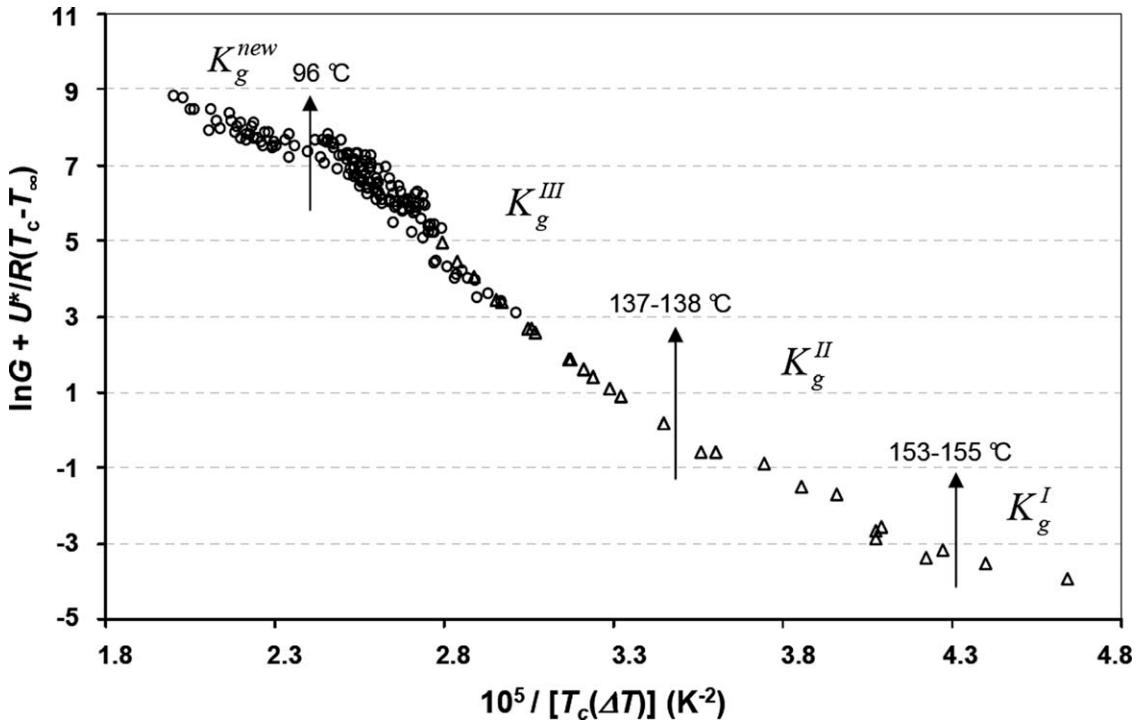

Figure 9 $\ln G + U^*/R(T_c - T_\infty)$ against $1/T_c(\Delta T)$ with G in μm/s. The different growth regimes are indicated.

Therefore, for a given growth regime, the plot of $\ln G + U^*/R(T_c - T_\infty)$ against $1/T_c(\Delta T)$ is a straight line, whose slope gives the value of K_g^i. Such a plot has been done for our polypropylene and can be seen in Figure 9 with its interpretation in terms of growth regimes. To establish it, the following values have been taken from Monasse and Haudin's article[44]: $T_m^0 = 208°C$ and $T_\infty = -51°C$. From Monasse's work,[44,45] a few points around 153°C and above could belong to Regime I. However, the high temperature range mainly corresponds to Regime II. The transition to Regime II occurs at about 137°C, in agreement with previous work.[44–46] Regime III is observed between 137 and 96°C. Below 96°C, the experimental points do no fit the straight line for Regime III. Such a situation was also described for polyethylene–octene copolymers.[47] Several possible causes have put forward: incorporation of comonomers leading to a decrease of the equilibrium melting temperature and to a lowering of the enthalpy of fusion, reduction of crowding in the interfacial regions causing a reduction of the fold surface energy. Apparently, these specific arguments do not apply to polypropylene.

The values of K_g^i and $\ln G_0^i$ for three regimes (II, III, "New") are reported in Table I. These values have not been calculated for Regime I, because of the lack of experimental data. The ratio K_g^{III}/K_g^{II} is equal to 2.05, which is close to the theoretical value of 2.[42,44–46] $K_g^{New}(3.61 \times 10^5\ K^2)$ is about two times smaller than $K_g^{III}(7.71 \times 10^5\ K^2)$: $K_g^{III}/K_g^{New} = 2.13$. The values of K_g^i are given with their average of absolute deviations (AAD) between the experimental results and the results recalculated from the fit:

$$\text{AAD} = 100\,\frac{\sum\left(\left(\ln G + \frac{U^*}{R(T_c - T_\infty)}\right)_{\text{exp}} - \left(\ln G_0^i - \frac{K_g^i}{T_c(\Delta T)}\right)_{\text{fit}}\right)}{\sum\left(\ln G + \frac{U^*}{R(T_c - T_\infty)}\right)_{\text{exp}}} \quad (20)$$

The summations are over all the experimental points. As this work is mainly concerned with the low-temperature behavior, the experimental points are less numerous in Regime II and consequently, the determination of the kinetic parameters is less accurate. Let us recall that the III→II transition has been the object of a detailed study in our group many years ago.[44]

TABLE I
Values of K_g^i and $\ln G_0^i$ for Three Regimes (II, III, "New")

Regimes	K_g^i (K^2) – AAD (%)	$\ln G_0^i$ (μm/s)
II	3.75×10^5 – 10.0	12.82
III	7.71×10^5 – 0.8	26.42
"New"	3.61×10^5 – 0.4	15.89

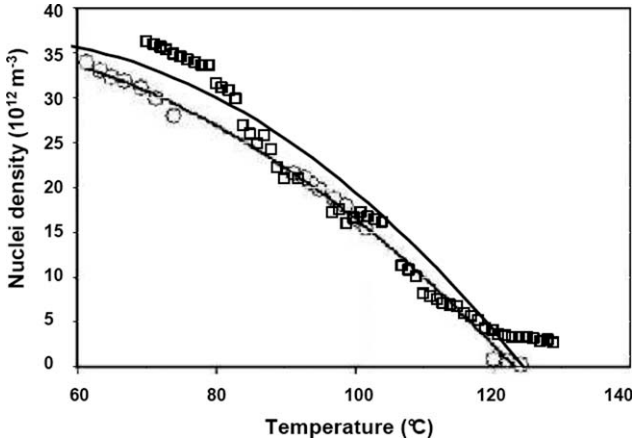

Figure 10 Estimates of the number of potential nuclei: Da Passano and Monasse[48] (circles); this work (squares).

Number of nuclei

It is possible to determine the number of activated nuclei by counting the number of spherulites. It has been done by Da Passano and Monasse[48] in a preliminary work, whose results are presented in Figure 10. In the case of instantaneous nucleation considered here, the number of activated nuclei per unit volume is the initial density of potential nuclei N_0. In this article, a different strategy is adopted to determine N_0. It is based on the approach proposed by Duffo[28] and already illustrated by Devisme et al.[27] If N_0 is constant, $\chi(T)$ is simply given by:

$$\chi(T) = \frac{4\pi}{3} N_0 \left[\int_T^{T_m^0} G(\Gamma)\, d\Gamma \right]^3 \tag{21}$$

Duffo[28] and Devisme et al.[27] then determine the value of N_0 at a given temperature T from the experimental value of $\chi(T)$:

$$N_0(T) = \frac{\chi(T)_{\text{experimental}}}{\frac{4\pi}{3}\left[\int_T^{T_m^0} G(\Gamma)\, d\Gamma \right]^3} \tag{22}$$

where $G(T)$ is given by eq. (18) for Regime III. The N_0 values obtained by this method are plotted in Figure 10 and fitted with the polynomial expression:

$$N_{0\text{calorimetry}} = A' + B'T + C'T^2 \tag{23}$$

with T in °C and $A' = 2.27 \times 10^{13}$, $B' = 5.86 \times 10^{11}$, and $C' = -6.17 \times 10^{9}$. These values, deduced from calorimetric measurements, are close to those obtained by direct microscopic observation, which validates our approach.

Discussion: extrapolation of overall kinetics

In the work of Devisme et al.,[27] the lowest temperature for the experimental determination of $\ln(\chi(T))$ was about 95°C. Therefore, the kinetic law was extrapolated to lower temperatures to be usable in the modeling of extrusion coating. To perform this extrapolation, the authors used the procedure described in the previous section to estimate the $N_0(T)$ curve and extrapolated it to 50°C. This extrapolated value was then used to calculate theoretical values of $\ln(\chi(T))$. Finally, both experimental and theoretical values of $\ln(\chi(T))$ were fitted using the same polynomial expression. In this work, the experimental domain has been extended down to 55°C by using more recent equipment. To cover the experimental range, some extrapolation is still necessary, but the domain of extrapolation is now more restricted, which should lead to more reliable data.

As a first remark, Figure 11 shows that the polynomial fit used in the experimental range diverges outside this range, which is not really surprising. There, more physically based extrapolations have been tried and compared to experimental data in Figure 12. They are based on the protocol of Devisme et al.[27] and differ by the assumptions

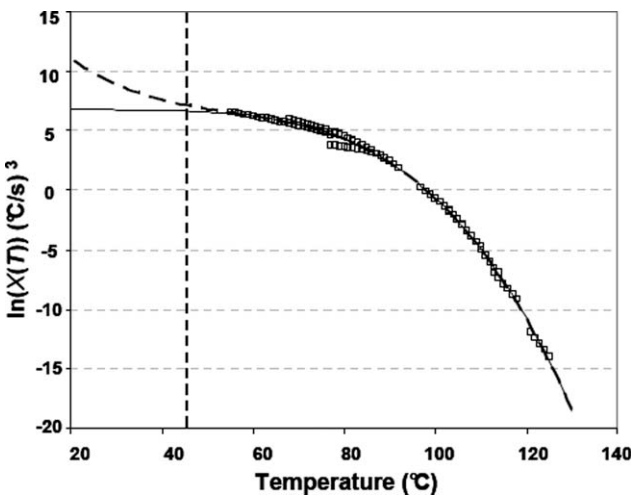

Figure 11 $\ln(\chi(T))$ versus temperature T. Symbols: Experimental results. Dashed line: polynomial fitting used in the experimental range and extended to lower temperatures. Full line: new polynomial fitting with $A = -1.38 \times 10^{-7}$, $B = 5.73 \times 10^{-6}$, $C = 1.93 \times 10^{-4}$, $D = -1.51 \times 10^{-2}$, and $E = 7.00$. Below 45°C (vertical line), the smectic phase is supposed to appear.

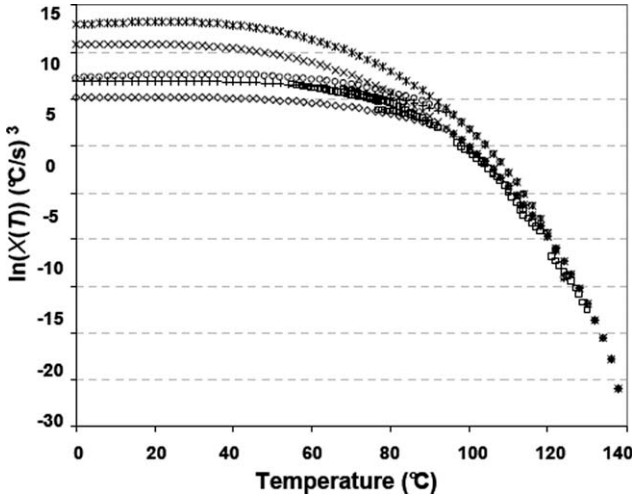

Figure 12 $\ln(\chi(T))$ versus temperature. Comparison between experimental (□) and theoretical data with $n = 3$:

1. Regime III with $N_0 = 2.93 \times 10^{12}$ nuclei/m^3 (x);
2. Regime III above 96°C and "new regime" below 96°C with $N_0 = 2.93 \times 10^{12}$ nuclei/m^3 (◇);
3. Regime III and "new regime" with $N_0 = 2.93 \times 10^{12}$ nuclei/m^3 above 96°C and $N_0 = 1.73 \times 10^{13}$ nuclei/m^3 below 96°C, respectively (+);
4. Regime III with $N_0(T)$ (*);
5. Regime III and "new regime" with $N_0(T)$ (○).

concerning nucleation and growth. These assumptions are the following:

1. Regime III with $N_0 = 2.93 \times 10^{12}$ nuclei/m^3;
2. Regime III above 96°C and "new regime" below 96°C with $N_0 = 2.93 \times 10^{12}$ nuclei/m^3;
3. Regime III and "new regime" with $N_0 = 2.93 \times 10^{12}$ nuclei/m^3 above 96°C and $N_0 = 1.73 \times 10^{13}$ nuclei/m^3 below 96°C;
4. Regime III with $N_0(T)$;
5. Regime III and "new regime" with $N_0(T)$.

Despite some difficulties in the connection of the curves below and above 96°C, due to the mode of calculation, it seems that the best fit, in terms of extrapolation to low temperatures, correspond to Case 3. Conversely, the results in the experimental range are not very good, as shown in Figure 13. Consequently, a mixed approach has been adopted: it consists in a purely mathematical fitting of experimental data taking into account extrapolation 3 at low temperatures. The whole temperature domain is represented by eq. (15) with new values of A, B, C, D, and E: $A = -1.38 \times 10^{-7}$, $B = 5.73 \times 10^{-6}$, $C = 1.93 \times 10^{-4}$, $D = -1.51 \times 10^{-2}$, and $E = 7.00$. This new function, which is also plotted in Figure 11, gives exactly the same results as the previous one in the experimental range. For instance, Figure 6 is exactly reproduced.

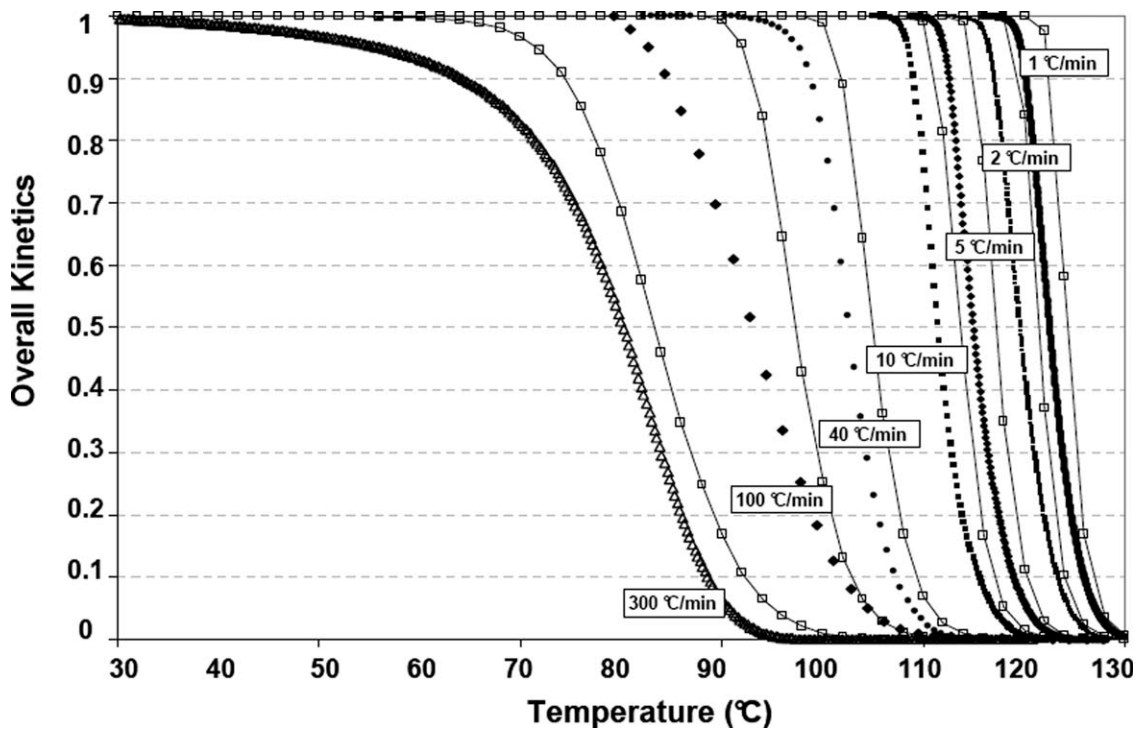

Figure 13 Comparison between overall kinetics for different $\dot{T}$ calculated with the new polynomial fit (full lines with squares) and experimental ones.

The kinetic law proposed above is valid as long as the α-crystalline phase of iPP is present. It is actually the case in all our experiments, by DSC as well as by optical microscopy. This was directly controlled by using the melting curves in DSC experiments, and checked after crystallization by X-ray diffraction for microscopy samples. Let us recall that the maximum cooling rates in DSC were of several hundreds of °C/min and that experiments with the « Polymer High Cooling—Optics » device were limited to about 2000°C/min. The smectic phase appears for cooling rates of the order of 100°C/s,[29,49] which corresponds to a crystallization temperature of about 45°C.[37,50] Consequently, our mathematical extrapolation has a physical meaning only above 45°C, and this physical frontier is indicated by a vertical line in Figure 11. The kinetic law should be completed by data concerning the smectic phase. To our knowledge, the only available data in the literature are those of De Santis et al.[37]

In this article, the determination of the overall kinetics law is based on Ozawas' equation, which is a simplified expression in principle valid for specific types of nucleation, like instantaneous nucleation. An Avrami exponent close to 3, obtained experimentally, can be interpreted in terms of instantaneous nucleation of 3D spherulites. This legitimates the use of Ozawa's approach. However, its remains an approximation, and it would be better to use the more general formulations presented in the section "THEORETICAL BACKGROUND," for instance Haudin–Chenot's equations. The latter model requires the temperature dependence of three physical parameters: the initial density of potential nuclei N_0, the activation frequency q of these nuclei, and the growth rate G. For the polymer under investigation, this determination has been done in a limited temperature range, 116–132°C,[10,11] where the temperature dependence can be described by exponential functions. Then, the values of the parameters were optimized by the genetic algorithm method.[51] The results obtained here show that obviously the variations of the number of potential nuclei cannot be described by an exponential law but by a smoother function. Therefore, it would be desirable extend our procedures of determination of N_0, q, and G to lower temperatures. In this work, a detailed characterization already exists for growth rate, and some data are available for nucleation. The « Polymer High Cooling—Optics » device could allow us to achieve a complete determination of the crystallization parameters, but it represents a considerable amount of work.

CONCLUSIONS

This work has first shown that by using new-generation commercial calorimeters, it is possible to measure the overall crystallization kinetics of isotactic polypropylene in a wide temperature range, including low crystallization temperatures. The cooling rates here were limited to 350°C/min, but by exploiting the maximum capacities of these setups, it should be possible to obtain data at higher cooling rates, i.e., at lower crystallization temperatures.

Then, the use of the prototype hot stage developed in our laboratory allowed us to obtain original results concerning the growth rate of α spherulites at low crystallization temperatures. These data do not correspond to the Regime III predicted by the theory, but to a "New" regime, which remains unexplained. Additionally, first determinations of the density of nuclei show a smooth evolution with temperature, with no apparent rupture in the nucleation behavior at low temperature.

The combination of all the experimental results and the test of different extrapolation procedures have led to an overall kinetics law valid in the whole domain of existence of the α-phase. This work should be completed by a kinetic law for the smectic phase, which appears below about 45°C. This should require new experiments involving other facilities, such as recently developed nanocalorimeters. A first approach could be to build this law from the few data existing in the literature.

A further step could be to apply the kinetic law for alpha and smectic phases to a process like extrusion coating, where only thermal effects are present. Of course, this type of approach would also be useful for injection molding, where high cooling rates are encountered. Nevertheless, in such a case, and especially in microinjection molding, flow effects should be taken into account, which would require other types of model experiments.

As discussed in the article, our kinetic law is based on Ozawa's formulation. In the future, it would be desirable to use more complete formulations, which need new experiments feasible with our prototype hot stage: depolarized light intensity measurements, counting of activated nuclei.

References

1. Avrami, M. J Chem Phys 1939, 7, 1103.
2. Avrami, M. J Chem Phys 1940, 8, 212.
3. Avrami, M. J Chem Phys 1941, 9, 177.
4. Evans, U. R. Trans Faraday Soc 1945, 41, 365.
5. Nakamura, K.; Watanabe, T.; Katayama, K.; Amano, T. J Appl Polym Sci 1972, 16, 1077.
6. Ozawa, T. Polymer 1971, 12, 150.
7. Billon, N.; Barq, P.; Haudin, J. M. Int Polym Process 1991, 6, 348.
8. Schneider, W.; Köppl, A.; Berger, J. Int Polym Process 1988, 2, 151.
9. Haudin, J. M.; Chenot, J. L. Int Polym Process 2004, 19, 267.
10. Monasse, B.; Smirnova, J.; Haudin, J. M.; Chenot, J. L. Int Polym Process 2004, 19, 275.

11. Boyer, S. A. E.; Grolier, J. P. E.; Yoshida, H.; Haudin, J. M.; Chenot, J. L. J Mol Liq 2009, 147, 24.
12. Ding, Z.; Spruiell, J. E. J Polym Sci B: Polym Phys 1996, 34, 2783.
13. Krumme, A. Polym Test 2004, 23, 29.
14. Becker, S.; Brisebourg, M.; Boyer, S. A. E. Int J Mater Form 2009, 2(Suppl 1), 853.
15. Haudin, J. M.; Boyer, S. A. E. Int J Mater Form 2009, 2(Suppl 1), 857.
16. Boyer, S. A. E.; Haudin, J. M. Polym Test 2009, 29, 445.
17. Märtson, T.; Ots, A.; Krumme, A., Lõhmus, A. Polym Test 2010, 29, 127.
18. Pijpers, T. F. J.; Mathot, V. B. F.; Goderis, B.; Scherrenberg, R. L.; van der Vegte, E. W. Macromolecules 2002, 35, 3601.
19. Vanden Poel, G.; Mathot, V. B. F. Thermochim Acta 2007, 461, 107.
20. Salmerón Sánchez, M.; Mathot, V. B. F.; Vanden Poel, G.; Gómez Ribelles, J. L. Macromolecules 2007, 40, 7989.
21. Pijpers, M. F. J.; Mathot, V. B. F. J Therm Anal Calorim 2008, 93, 319.
22. Mathot, V. B. F. J Therm Anal Calorim 2010, 102, 403.
23. Adamovsky, S. A.; Minakov, A. A.; Schick, C. Thermochim Acta 2003, 403, 55.
24. Adamovsky, S. A.; Schick, C. Thermochim Acta 2004, 415, 1.
25. Minakov, A. A.; Adamovsky, S. A.; Schick, C. Thermochim Acta 2005, 432, 177.
26. Gradys, A.; Sajkiewicz, P.; Minakov, A. A.; Adamovsky, S.; Schick, C.; Hashimoto, T.; Saijo, K. Mater Sci Eng 2005, A413–A414, 442.
27. Devisme, S.; Haudin, J. M.; Agassant, J. F.; Rauline, D.; Chopinez, F. Int Polym Process 2007, 22, 90.
28. Duffo, P. Ph.D. Thesis, Ecole des Mines de Paris: France, 1990.
29. Piccarolo, S. J Macromol Sci Phys 1992, B31, 501.
30. Piorkowska, E.; Galeski, A.; Haudin, J. M. Prog Polym Sci 2006, 31, 549.
31. Piorkowska, E.; Galeski, A. J Appl Polym Sci 2002, 86, 1363.
32. Jay, F.; Monasse, B.; Haudin, J. M. Int J Form Proc 1998, 1, 75.
33. Seo, Y.; Kim, J.; Kim, K. U.; Kim, Y. C. Polymer 2000, 41, 2639.
34. Devaux, N.; Monasse, B.; Haudin, J. M.; Moldenaers, P.; Vermant, J. Rheol Acta 2004, 43, 210.
35. Hieber, C. A. Polymer 1995, 36, 1455.
36. Magill, J. H. Polymer 1962, 3, 35.
37. De Santis, F.; Adamovsky, S.; Titomanlio, G.; Schick, C. Macromolecules 2007, 40, 9026.
38. Nakamura, K.; Shimizu, S.; Umemoto, S.; Thierry, A.; Lotz, B.; Okui, N. Polym J 2008, 40, 915.
39. Janeschitz-Kriegl, H. Macromolecules 2006, 39, 4448.
40. Lauritzen, J. I., Jr.; Hoffman, J. D. J Res Natl Bur Stand A 1960, 64, 73.
41. Hoffman, J. D.; Frolen, L. J.; Ross, G. S.; Lauritzen, J. I., Jr. J Res Natl Bur Stand A 1975, 79, 671.
42. Hoffman, J. D. Polymer 1983, 24, 3.
43. Hoffman, J. D.; Miller, R. L. Polymer 1997, 38, 3151.
44. Monasse, B.; Haudin, J. M. Colloid Polym Sci 1985, 263, 822.
45. Monasse, B. Ph.D. Thesis, Université Claude Bernard Lyon 1: France, 1987.
46. Clark, E. J.; Hoffman, J. D. Macromolecules 1984, 17, 878.
47. Wagner, J.; Abu-Iqyas, S.; Monar, K.; Phillips, P. J. Polymer 1999, 40, 4717.
48. Da Passano, E.; Monasse, B. Research Report, MINES ParisTech: France, 2006.
49. De Santis, F.; Adamovsky, S.; Titomanlio, G.; Schick, C. Macromolecules 2006, 39, 2562.
50. Cavallo, D.; Azzurri, F.; Floris, R.; Alfonso, G. C.; Balzano, L.; Peters, G. W. Macromolecules 2010, 43, 2890.
51. Smirnova, J.; Silva, L.; Monasse, B.; Haudin, J. M.; Chenot, J. L. Eng Comput 2007, 24, 486.